Journal of
Mechanical
Science and
Technology

Journal of Mechanical Science and Technology 21 (2007) 2082~2090

Statistical energy analysis of non-resonant response of isotropic and orthotropic plates

Chieh-Yuan Cheng*, Rong-Juin Shyu and Der-Yuan Liou

Department of Systems Engineering and Naval Architecture, National Taiwan Ocean University, Keelung, Taiwan

(Manuscript Received January 26, 2007; Revised July 5, 2007; Accepted July 6, 2007)

Abstract

The conventional SEA model considers only the resonant part of the structural response to an acoustic excitation. Therefore, this study investigates non-resonant responses of isotropic and orthotropic plates to acoustically induced vibrations in a reverberation chamber. A modified SEA model is introduced to predict the non-resonant plate response. The estimated non-resonant and resonant responses are then compared with those obtained experimentally, and good agreement is observed for isotropic and orthotropic plates. For an isotropic plate with a small dissipation loss factor, when the non-resonant part is ignored, the estimated response can lead to significant errors at frequencies near and above the critical frequency, while large errors may occur at frequencies below the critical frequency for an orthotropic plate with a high dissipation loss factor. The experimental study indicates that the non-resonant response component should be included in the estimated responses to enhance predictive accuracy.

Keywords: Non-resonant response; Orthotropic plate; Statistical energy analysis.

1. Introduction

In recent decades, statistical energy analysis (SEA) has been considered to be a suitable framework for analyzing and solving vibro-acoustic problems. Statistical energy analysis assumes that energy flow between subsystems is caused by resonant structural or acoustic modes [1]. When excited acoustically, conventional SEA models cannot predict the non-resonant response of a structure [2-4]. A non-resonant response, also known as a forced response, is a response of structures that vibrate when impacted by sound waves. A resonant response is associated with structural modes that are caused by the interaction of free bending waves with a structure's boundaries. Therefore, both non-resonant and resonant responses contribute to an acoustically induced vibration response.

*Corresponding author. Tel.: +886 2246 22192, Fax.: +886 2246 24634
E-mail address: vibnoise@gmail.com

However, few studies have estimated the non-resonant structural response to acoustic excitation using SEA [4, 5], since Renji et al. [4] proposed a direct non-resonant coupling loss factor between a room and a partition. A modified SEA (MSEA) model has thus been constructed to estimate the non-resonant energy transfer between rooms and partitions. Renji et al. considered the transmission of sound through a single-leaf aluminum plate as a numerical example. Cheng and Shyu [5] developed this idea further to investigate the transmission of sound through double and triple leafs. They used a non-resonant coupling loss factor between a cavity and a partition to estimate non-resonant energy transfer. It was found that the non-resonant response of an aluminum plate could be significant for resonant responses at frequencies near and above the critical frequency, for an assumed dissipation loss factor of the aluminum plate of 0.01 for all frequencies [4, 5]. The assumption of a dissipation loss factor influences the resonant and non-resonant contributions to the

response of plates, which will be discussed later. Renji et al. [6] also conducted an experiment in which they subjected an aluminum plate to acoustic excitation in a reverberation chamber, to verify the MSEA model [4]. In their study, the estimated response of the aluminum plate showed large errors at frequencies near and above the critical frequency when the non-resonant response was ignored. To date, some works have studied the non-resonant response of isotropic aluminum plates with tiny dissipation loss factors; however, few have been conducted on orthotropic plates with high dissipation loss factors, to the authors' knowledge.

This work studies the non-resonant response of orthotropic plates to acoustic excitation, as well as the effects of the dissipation loss factor for the non-resonant response of metal plates. Since fiber-reinforced plastic (FRP) plates have orthotropic characteristics and higher damping values than aluminum plates, the non-resonant response contribution of FRP plates differs from that of isotropic metal plates. This work measures the structural responses of aluminum and FRP plates that are subjected to acoustic excitation in a reverberation chamber. Experimental data are compared with structural responses of the plates that are predicted by using the MSEA [4]. The modified SEA model is expected to improve predicted structural responses of the plates. Besides, reverberation time of the chamber was also measured to calculate the chamber's absorption coefficient. The total loss factor of each plate was also measured to calculate the dissipation loss factor.

2. Experiment

Figs. 1(a) and 2(b) present the setup of the acoustically induced vibration test for an aluminum plate and an FRP plate, respectively. These two plates were hung in a reverberation chamber during the test. White noise generated by a non-directional loudspeaker was adopted to excite acoustically the test plate, and the acceleration responses of the plates were measured.

Fig. 2 presents the dimensions and plan view of the reverberation chamber, which is an irregularly shaped concrete building with a volume of 204 m^3 and a surface area of 202 m^2. The temperature and relative humidity during the test were 21°C and 70%, respectively. Under these conditions, the density of air was 1.18 kg/m^3 and the speed of sound was 344 m/s. The first test structure, an aluminum plate of type 1050, was 1.245 m × 1.485 m in area and 3 mm thick. The material properties were as follows [5]: Young's modulus $E = 7.1\times10^{10}$ Pa; Poisson ratio $\nu = 0.3$, and density $\rho = 2700$ kg/m^3. The modal density of the isotropic aluminum plate at frequency f was calculated as 0.2 by using the following equation [1].

$$n(f) = (A/2)(m/D)^{1/2}, \tag{1}$$

where A is the area; m is the mass per unit area, and D is the flexural rigidity. The critical frequency of the plate was calculated to be 4045 Hz [1]

$$f_c = \frac{c^2}{2\pi}\sqrt{\frac{m}{D}}. \tag{2}$$

The second test structure, an orthotropic plate made of FRP, was 1.245 m × 1.485 m in area and 2.6 mm thick. The material properties of this orthotropic plate were as follows [5]: Young's modulus in the plane direction $E_x = 2.5\times10^{10}$ Pa and $E_y = 1.4\times10^{10}$ Pa; Poisson ratio $\nu_{xy} = 0.25$, and density $\rho = 1630$ kg/m^3. The modal density of the FRP plate at frequency f was calculated as 0.36 [1], using

$$n(f) = (A/4)\left(\frac{m}{D_x}+\frac{m}{D_y}\right)^{1/2}, \tag{3}$$

where D_x and D_y are the flexural rigidity of the orthotropic plate in relation to in-plane axes (x-axis and y-axis). The orthotropic plate is characterized by a range of critical frequencies that depend on the direction of propagation of the bending wave in the plate. According to Eq. (2), the lowest critical frequency of the FRP plate is f_{c1}=6293 Hz, and the highest critical frequency is f_{c2}=8380 Hz.

A white noise signal that is generated by the built-in signal generator of B&K 3560C was amplified to drive the non-directional loudspeaker. The sound pressure level (SPL) was measured by five B&K 4190 microphones, which were placed randomly in the reverberation chamber, as shown in Fig. 1, to calculate the spatial average SPL. Six B&K 4374 miniature accelerometers, each weighing 0.65 gram, were placed randomly on the plate to measure acceleration and thus determine the acoustically induced plate vibration (Fig. 3). Fig. 4 presents the measurement setup for capturing sounds and vibrations. Two B&K 3560C spectrum analyzers, connected in a network, were adopted to analyze 11 channels of signals

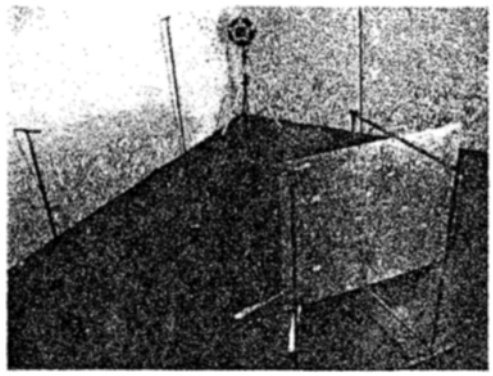

Fig. 1(a). An aluminum plate in the reverberation chamber.

Fig. 1(b). An FRP plate in the reverberation chamber.

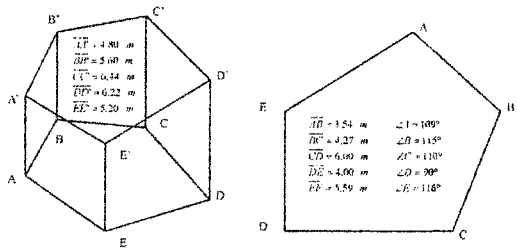

Fig. 2. Dimensions of the reverberation chamber.

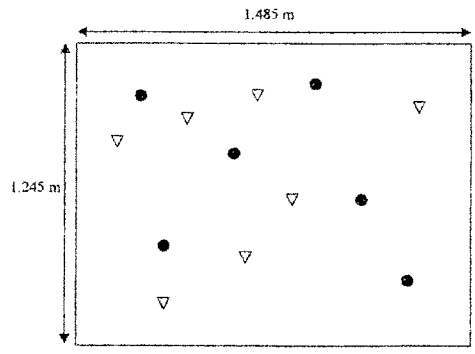

Fig. 3. Accelerometer(●) and hammer impact(▽) locations on the plate.

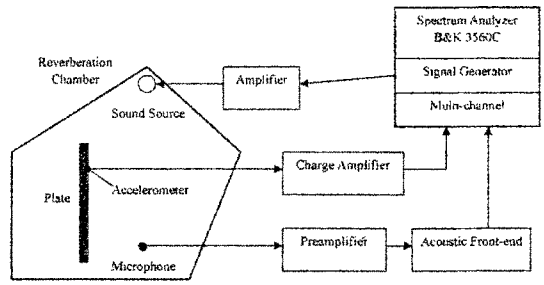

Fig. 4. Acoustic-induced vibration measurement setup.

in one-third octave bands, ranging from 400–8000 Hz for the aluminum plate and 400–12500 Hz for the FRP plate. Results above 400 Hz were presented to eliminate inaccuracies in radiation resistance at low frequencies, and to fulfill the SEA assumptions for sufficient mode counts in the lowest frequency band [6]. The 400 Hz one-third octave band for the aluminum and FRP plates had 18 and 33 modes, respectively.

Figs. 5(a)-5(d) present the spectra of SPL and the plate vibration, as displayed on a B&K 3560C spectrum analyzer. Tables 1 and 2 present the measured spatial average SPL for the aluminum plate and the FRP plate. Figs. 6 and 7 present the spatial average for acceleration levels for the two plates. The reverberation time of the chamber and the total loss factor of the plates were measured to estimate the absorption coefficient of the chamber and the dissipation loss factor of the plates. Tables 1 and 2 list the estimated absorption coefficients for various plates. For brevity, details of the experiments for reverberation time are not provided here as they are given in ISO 3382. The power injection method was utilized to measure the total loss factor η_t of the plate at circular frequency ω. That is, [7, 8]

$$\eta_t = \frac{1}{E_i^n} = \frac{P_i}{\omega \cdot E_i}, \tag{4}$$

where E_i represents the space and frequency-averaged energy of the vibration of the plate; P_i is the power input, and E_i^n is the normalized energy level. Once the input power and the energy of the plate vibration have been measured, the total loss factor of the plate can be experimentally determined. Fig. 8 presents the experimental arrangement for the loss factor measurements. An impact hammer was used to excite the plate at seven randomly selected points (Fig. 3). Six accelerometers were used to

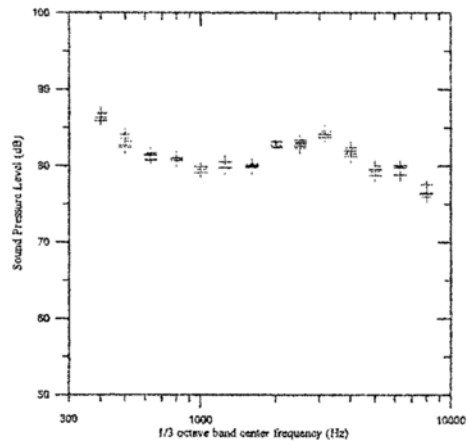

(a) SPL spectrum (aluminum plate)

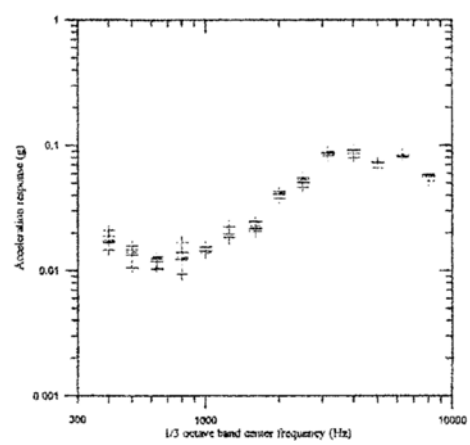

(b) Acceleration spectrum (aluminum plate)

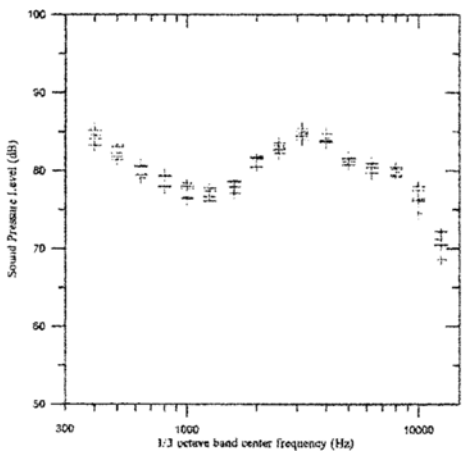

(c) SPL spectrum (FRP plate)

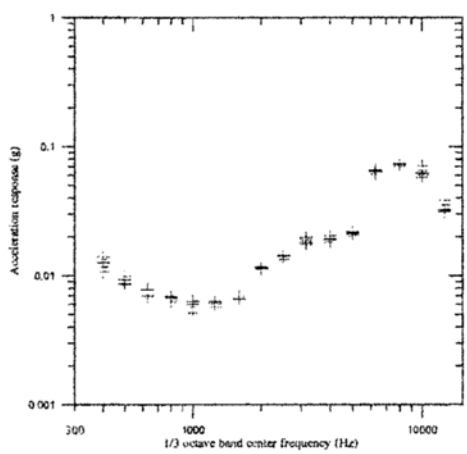

(d) Acceleration spectrum (FRP plate)

Fig. 5. Spectrums of the SPL and the plate vibration level.

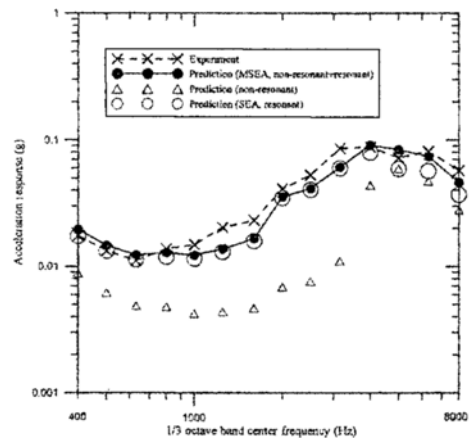

Fig. 6. Acceleration responses of the aluminum plate.

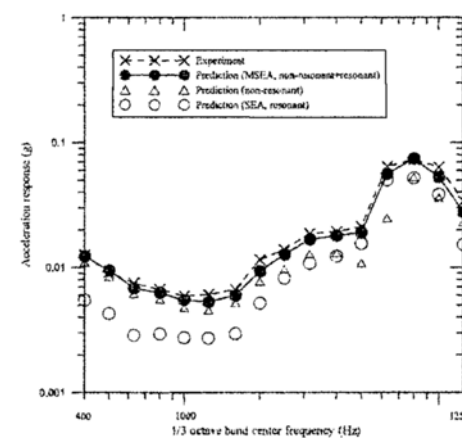

Fig. 7. Acceleration responses of the FRP plate.

Table 1. Structural responses of the aluminum plate.

1/3 octave band	SPL	Absorption coefficient	Vibration response(dB)			Vibration level difference(dB)
center frequency(Hz)	in chamber (dB)	of chamber	Experiment	SEA	Modified SEA	|SEA-Modified SEA|
400	86.4	0.012	84.7	84.6	85.6	1.0
500	83.3	0.014	82.3	82.3	83.1	0.8
630	81.2	0.017	80.7	80.9	81.7	0.8
800	80.9	0.017	82.6	81.3	82.0	0.7
1000	79.8	0.018	83.3	81.0	81.6	0.6
1250	79.9	0.020	86.0	82.1	82.6	0.5
1600	80.0	0.021	87.1	83.8	84.2	0.4
2000	82.8	0.023	92.1	90.7	90.8	0.1
2500	82.9	0.026	94.3	91.9	92.1	0.2
3150	84.1	0.030	98.5	95.4	95.5	0.1
4000	81.8	0.037	98.7	97.8	99.0	1.2
5000	79.4	0.048	97.0	95.2	98.3	3.1
6300	79.7	0.068	98.0	94.9	97.2	2.3
8000	76.6	0.089	95.0	91.2	93.1	1.9

* dB reference for vibration response is 10^{-5} m/s^2

Table 2. Structural responses of the FRP plate.

1/3 octave band	SPL	Absorption coefficient	Vibration response(dB)			Vibration level difference(dB)
center frequency(Hz)	in chamber (dB)	of chamber	Experiment	SEA	Modified SEA	|SEA-Modified SEA|
400	84.5	0.013	81.8	74.6	81.6	7.0
500	82.4	0.014	79.1	72.5	79.4	6.9
630	79.9	0.016	77.3	69.0	76.5	7.5
800	78.8	0.019	76.3	69.2	75.8	6.6
1000	77.5	0.019	75.3	68.6	74.6	6.0
1250	77.2	0.020	75.5	68.5	74.4	5.9
1600	78.2	0.021	76.3	69.3	75.4	6.1
2000	81.5	0.023	81.1	74.1	79.2	5.1
2500	83.0	0.025	82.7	78.2	81.9	3.7
3150	85.2	0.027	85.3	80.5	84.3	3.8
4000	84.6	0.031	85.6	81.6	84.9	3.3
5000	81.4	0.038	86.4	83.7	85.4	1.7
6300	80.1	0.049	96.0	93.9	94.8	0.9
8000	80.0	0.060	97.1	94.2	97.3	3.1
10000	76.6	0.087	95.9	91.5	94.3	2.8
12500	70.6	0.105	90.4	83.5	88.7	5.2

* dB reference for vibration response is 10^{-5} m/s^2

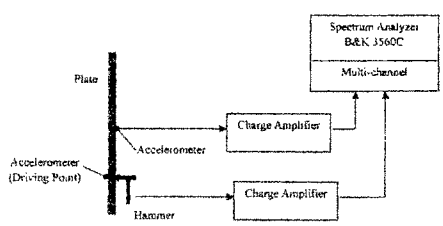

Fig. 8. Total loss factor measurement setup of the aluminum and FRP plates.

measure the energy of the plate vibration; while the other one locating with movement of the impact point was used to estimate the input power of the driving point. Figs. 9 and 10 plot total loss factor measurements of various plates. Since an impact hammer with a steel tip was used to measure the total loss factor, the frequency response of the impact energy was limited to high frequency range. The resulting total loss factors at frequencies above 2000 Hz, shown in

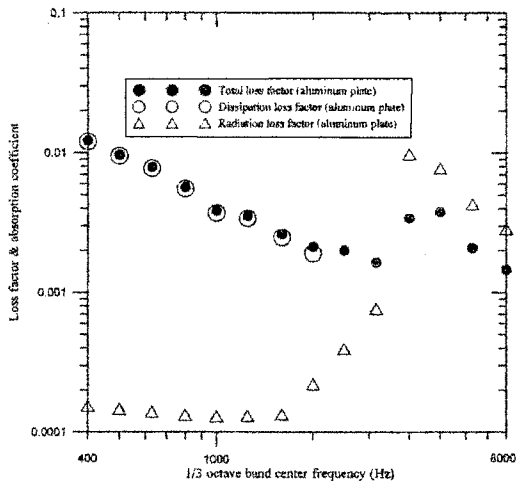

Fig. 9. Different loss factors of the aluminum plate.

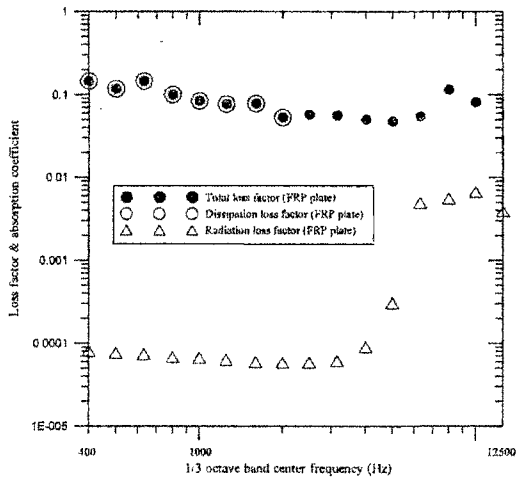

Fig. 10. Different loss factors of the FRP plate.

Figs. 9 and 10, are for reference only. The radiation loss factor was subtracted from the total loss factor to determine the dissipation loss factors of the two plates. The radiation loss factor was determined from the plate radiation efficiency. Hence,

$$\eta_r = \frac{\rho_a c \sigma}{\omega m}, \tag{5}$$

where ρ_a is the density of air, and c is the speed of sound in air. The radiation efficiency of a simply supported plate, σ, was computed by using the equations given by Leppington et al. [9]. In this work, the plate boundaries are free. A factor of 0.5, as suggested by Renji et al. [6, 10], up to a frequency of $\frac{f_c}{2}$, was applied to the radiation efficiency to take into account the effect of the free condition. Fig. 9 plots the estimated theoretical radiation and dissipation loss factors of the aluminum plate. Since orthotropic plates have a critical frequency region, the radiation efficiency of the orthotropic plate, as suggested by Craik [3], was estimated herein by taking the average radiation efficiency of two isotropic plates—one with the lowest critical frequency (6293 Hz) and the other one with the highest critical frequency (8380 Hz). Fig. 10 plots the estimated theoretical radiation and dissipation loss factor of the FRP plate.

3. Results and discussion

3.1 Theoretical model of a panel that is hung in a reverberation room

Renji et al. [4] proposed the MSEA model of a plate that is hung in a diffuse acoustic field to estimate its resonant and non-resonant responses (Fig. 11). Their model consists of three subsystems - chamber (subsystem 1), resonant response of plate (subsystem 2), and non-resonant response of plate (subsystem 3). The indirect coupling loss factor, η_{31}, from the plate to the chamber, and the indirect coupling loss factor, η_{13}, from the chamber to the plate, are calculated by using the following equations:

$$\eta_{31} = 2\rho_a c / m\omega, \tag{6}$$

$$\eta_{13} = (\alpha_d + 2\tau) Ac / 4\omega V_1, \tag{7}$$

where $\alpha_d = \omega m \eta \tau / \rho_a c$ is the sound power dissipation coefficient; τ is the sound power transmission coefficient of the plate; η is the dissipation loss factor of the plate, and V_1 is the volume of the chamber. The power balance of these three subsystems, shown in Fig. 11, is given by the following equation:

$$\begin{Bmatrix} \pi_1 \\ 0 \\ 0 \end{Bmatrix} = \omega \begin{bmatrix} \eta_1 + \eta_{12} + \eta_{13} & -\eta_{21} & -\eta_{31} \\ -\eta_{12} & \eta + \eta_{21} & 0 \\ -\eta_{13} & 0 & \eta + \eta_{31} \end{bmatrix} \begin{Bmatrix} E_1 \\ E_2 \\ E_3 \end{Bmatrix}, \tag{8}$$

where π_i is the power input to the chamber; η_1 is the internal loss factor of the chamber, and E_i is the mean energy of subsystem i. For chamber sound pressure p_1, the chamber energy is given by

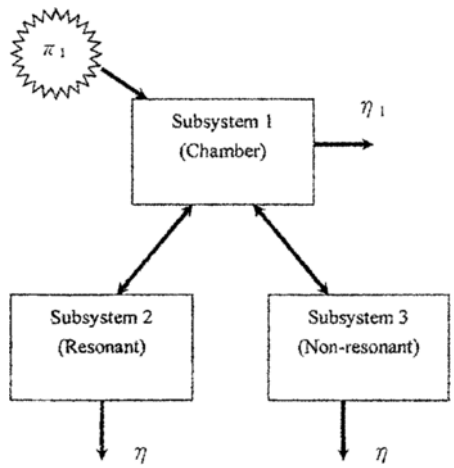

Fig. 11. A modified SEA model.

$$E_1 = (p_{1,rms}^2 / \rho_a c^2) V_1 . \tag{9}$$

From Eq. (8), the resonant vibration energy of the plate is given by

$$E_2 = \frac{n_2}{n_1}(1 + \frac{\omega m \eta}{\rho_a c \sigma})^{-1} E_1 , \tag{10}$$

where n_1 is the modal density of the acoustic chamber and n_2 is the modal density of the plate. The non-resonant vibration energy of the plate becomes

$$E_3 = \frac{\tau m A}{4 \rho_a V_1} E_1 . \tag{11}$$

The sound power transmission coefficient of a stiff isotropic plate with critical frequency f_c is given by [11]:

$$\tau^{-1} = \{1 + \eta a \cos\theta \sin^4\theta (f/f_c)^2\}^2 + \{a \cos\theta (1 - (f/f_c)^2 \sin^4\theta)\}^2 , \tag{12}$$

where $a = m\omega / 2\rho_a c$ and θ is the angle of incidence. For an orthotropic plate, the sound power transmission coefficient is estimated from [12]

$$\tau^{-1} = \{1 + \eta a \cos\theta \sin^4\theta (\frac{f}{f_{c1}} \cos^2\vartheta + \frac{f}{f_{c2}} \sin^2\vartheta)^2\}^2 + \{a \cos\theta [1 - (\frac{f}{f_{c1}} \cos^2\vartheta + \frac{f}{f_{c2}} \sin^2\vartheta)^2 \sin^4\theta]\}^2 , \tag{13}$$

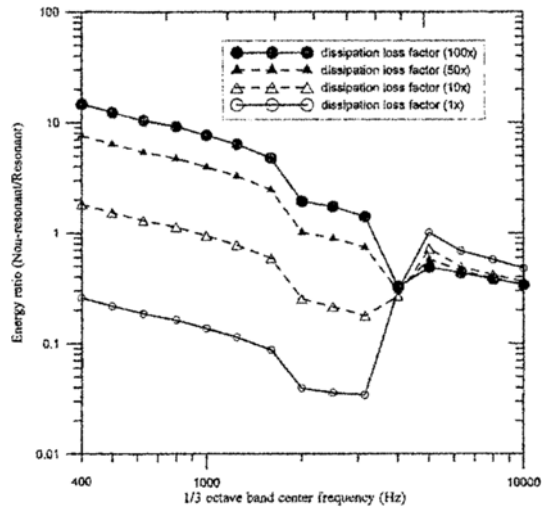

Fig. 12. The influence of increasing dissipation loss factor on vibration energy ratio (non-resonant/resonant) for aluminum plate.

where θ and ϑ are the angles of incidence. Eqs. (10) and (11) reveal that the dissipation loss factor of the plate influences the vibration energy of the non-resonant and resonant responses. The resonant vibration energy is proportional to the damping factor whereas the non-resonant vibration energy is not [3]. For the aluminum plate, the effect of an increase in the damping value on the resonant vibration energy is more significant than that on the non-resonant vibration energy.

3.2 Numerical results for aluminum plate

This section presents numerical results for an aluminum plate obtained with the MSEA model. Table 1 presents the SPL in the chamber and the absorption coefficient. Since the dissipation loss factor obtained from the experimental data can involve errors that exceed 2000 Hz, the dissipation loss factor is estimated from the following equation for $80\ \text{Hz} \le f \le 2500\ \text{Hz}$ [6, 13, 14].

$$\eta = 1.8 / (f^{0.87}) . \tag{14}$$

For frequencies above 2500 Hz, the dissipation loss factor was 0.002. Fig. 6 shows that the predicted non-resonant and resonant responses of the aluminum plate match the experimental results closely. This figure also shows that non-resonant response is significant when compared with the resonant response at frequencies near and above the critical frequency;

however, the non-resonant response is much lower than the resonant response below the critical frequency. That is, the non-resonant response contribution to plate vibration increases with frequency. The last column in Table 1 indicates that when the non-resonant response is ignored, the estimated response exhibits a significant error at frequencies above the critical frequency (3.1 dB at 5000 Hz), while the non-resonant response is negligible below the critical frequency. This result is in complete agreement with the experimental results of Renji et al. [4, 6] . The situation changes as the plate dissipation loss factor increases, as shown in Fig. 12. Numerical results reveal that the non-resonant response is higher than the resonant response at low frequencies and cannot be neglected. This result is not found in the earlier study.

3.3 Numerical results for FRP plate

This section discusses the response of the orthotropic FRP plate with a high dissipation loss factor. Table 2 presents the chamber SPL and the absorption coefficient. The dissipation loss factor of the FRP plate is based on experimental data for frequencies below 2000 Hz (Fig. 10) and is assumed to be 0.03 at frequencies above 2500 Hz. Fig. 7 plots the predicted plate non-resonant and resonant responses, which are strongly consistent with the experimental results.

The non-resonant response exceeds the resonant response at frequencies below 4000 Hz and greater than 8000 Hz (Fig. 7). The final column in Table 2 presents the differences between then estimated acceleration response with and without consideration of the non-resonant response. The differences are 7.5 dB at 630 Hz and 5.2 dB at 12500 Hz (Fig. 7 and Table 2), and increase markedly as the frequency declines below the critical frequency.

Based on the differences between the aluminum plate and the FRP plate at frequencies below the critical frequency, the non-resonant structural response of the FRP plate is higher than the resonant structural response, while the non-resonant structural response of the aluminum plate is lower than the resonant structural response. When the non-resonant structural response is neglected, the responses of the FRP plate estimated by using the conventional SEA are significantly lower than the measured results; however, the non-resonant structural response of the aluminum plate is negligible. At frequencies above the critical frequency, the non-resonant structural response of two plates is significant.

4. Conclusions

This work studied the structural responses of an aluminum plate and an FRP plate to acoustic excitation, by comparing experimental results with theoretical predictions. A modified SEA model predicted a structural response, including the non-resonant response, which agrees closely with the experimental results obtained for both plates. The dissipation loss factors of the two plates were determined in an experiment using the power injection method. The non-resonant structural response of the aluminum plate was as significant as the resonant response at frequencies near and above the critical frequency; however, the non-resonant response was insignificant at frequencies below the critical frequency. Increasing the dissipation loss factor of the plate may strengthen the non-resonant response rather than the resonant response below the critical frequency. The FRP plate had a high dissipation loss factor, and its non-resonant response exceeded the resonant response at frequencies below and above the critical frequencies. This work concludes that the non-resonant response component should be included in the estimated response calculation to improve predictions for both isotropic aluminum and orthotropic FRP plates.

References

[1] R. H. Lyon, Statistical Energy Analysis of Dynamical Systems: Theory and Applications, Cambridge, MA: MIT Press, (1975).

[2] M. P. Norton, Fundamentals of Noise and Vibration Analysis for Engineers, Cambridge University Press, New York, (1989).

[3] R. J. M. Craik, Sound Transmission Through Buildings Using Statistical Energy Analysis, Gower Publishing Limited, UK, (1996).

[4] K. Renji, P. S. Nair and S. Narayanan, Non-resonant response using statistical energy analysis, *Journal of Sound and Vibration.* 241 (2) (2001) 253-270.

[5] C. Y. Cheng and R. J. Shyu, Sound transmission of double and triple leafs using statistical energy analysis, *Journal of Taiwan Society of Naval Architects and Marine Engineers*. 25 (1) (2006) 1-6.

[6] K. Renji, P. S. Nair and S. Narayanan, Response of

a plate to diffuse acoustic field using statistical energy analysis, *Journal of Sound and Vibration*. 254 (3) (2002) 523-539.

[7] D. A. Bies and S. Hamid, In situ determination of loss and coupling loss factors by the power injection method, *Journal of Sound and Vibration*. 70 (2) (1980) 187-204.

[8] K. D. Langhe and P. Sas, Statistical Analysis of the Power Injection Method, *Journal of the Acoustical Society of America*. 100 (1) (1996) 294-303.

[9] F. G. Leppington, E. G. Broadbent and K. H. Heron, The acoustic radiation efficiency of rectangular panels, *Proceedings of the Royal Society of London*. 382 (1982) 245-271.

[10] K. Renji and P. S. Nair, On acoustic radiation resistance of Plates, *Journal of Sound and Vibration*. 212 (4) (1998) 583-598.

[11] F. Fahy, Sound and Structural Vibration: Radiation, Transmission and Response, Academic Press, London, (1985).

[12] C. H. Hansen, Sound Transmission Loss of Corrugated Panels, *Noise Control Engineering Journal*. 40 (2) (1993)187-197.

[13] R. J Cummins and I. R. Farrow, Study of the Evolution of Structural Acoustic Design Guides, ESA CR(P)-1609, Volume 1. (1981).

[14] D. C. G. Eaton, Structural Acoustics Design Manual, ESA PSS-03-1201, Issue 1. (1987).